RSC Advances

ROYAL SOCIETY OF CHEMISTRY

www.rsc.org/advances

Theranostics fluorescent silica encapsulated magnetic nanoassemblies for *in-vitro* MRI imaging and hyperthermia

Sunil Kumar[a], Amita Daverey[b,c] Vahid Khalilzad-Sharghi[d], Niroj K. Sahu[b], Srivatsan Kidambi[c], Shadi F. Othman[d] and Dhirendra Bahadur[b]*

*[a]Department of Chemical Engineering [b]Department of Metallurgical Engineering and Materials Science, Indian Institute of Technology Mumbai-400076,India.[c]Department of Chemical and Bimolecular Engineering, [d]Department of Biological Systems Engineering, University of Nebraska, Lincoln, NE-68588. USA.*E-mail: dhirenb@iitb.ac.in Tel: +9122-25767632, Fax: +91 22 2576 3480.*

Introduction

The recent advances in nanotechnology have made significant progress in the treatment of various diseases including cancer. A potential theranostic nanosystem can be evaluated based on their ability to monitor and deliver the therapeutic molecules at the specific site of tumours. Therefore, the capability of imaging and targeted therapy at specific site are the two important criterion for cancer theranostics.[1]In the past few years, several nano-systems have been proposed as potential theranostics for cancer.[1] Amongst these, super-paramagnetic iron oxide nanoparticles (SPIONs) or their derivates have emerged as a better option due to their unique properties of magnetic manipulation, T_2 contrast agent in magnetic resonance imaging (MRI) and ability to generate localized homogeneous heat at the sites of tumour on exposure to AC magnetic field.[2-5]It provides an opportunity to use them for hyperthermia treatment at localised site of tumour without affecting normal healthy cells. It has been shown that the theranostic efficacy of SPIONs can be enhanced if conjugated with optical nano modalities such as organic dyes, semiconductor quantum dots (Q-dots) etc [6-8]

These types of multifunctional theranostic modalities not only help in early diagnosis of malignant tissue by MRI or other imaging techniques, but also help in monitoring the progress of induced therapies by optical imaging. Various organic-inorganic hybrid nanosystems have been used to integrate the optical imaging nanomodalities with MNPs[1,9,10]. Among these, silica has several advantages such as easy synthesis, biocompatibility, high labeling and encapsulation efficiency for optical nanomodalities or as a therapeutic agent.[8,11] Mitchell *et al* demonstrated the biodegradation of silica nanoparticles in combination of MNPs due to the presence of iron chelating agents in serum.[12] Thus, silica encapsulated MNPs can be used without any toxicity issue for clinical application.There have been several reports describing the fabrication of semiconductor quantum dot (QDs)[13] or lanthanides luminescent nanoparticles (LNPs) within silica matrix.[14] The toxicity issue with QDs and difficulties in synthesis of LNPs in silica matrix, hamper their practical applicability as a potential fluorescent cancer theranostic nanosystems. The various organic fluorescent dyes such as fluorescein isothiocyanate (FITC) or rhodamine-B isothiocyanate (RITC) have been used as an alternate biocompatible entity for optical imaging.[15,16]

Recently, Food and drug administration of USA (FDA) approved the dye doped silica nanoparticle known as Cornell-dot or C-dot (<10 nm) for bio-imaging in clinical applications.[17] There are many reports describing the synthesis of dye doped or embeded magnetic-silica nanoparticles as nanoparobes for cancer theranostics.[14,15] But, the issue with them is their bigger size, dispersibility and stability in aqueous solutions, which create a problem for *in-vivo* applications at a clinical level. It remains a great challenge to synthesize uniform and monodisperse, biocompatible and biodegradable, small size (below100nm) silica based multifunctional theranostic nanosystem composed of MNPs

with fluorescence property and high colloidal stability. In this present study, we have synthesized a highly monodisperse and precisely size-controllable (<100nm) manganese ferrite nanoassemblies (MNAs) through a facile solvothermal method. The MNAs were encapsulated by two layers of silica shell. The inner silica shell infused with organic fluorescence dyes Rhodamine-B-isothiocyanate (RITC), whereas the outer silica shell, without dye, helps to prevent photo-bleaching and enhance photo-stability denoted as MNAs@Dye-SiO2@SiO2. The MNAs@Dye-SiO2@SiO2 form a very good colloidal dispersion in water and exhibit a superparamagnetic feature with a high magnetization. The theranostic efficacy of MNAs@Dye-SiO2@SiO2 was evaluated *in-vitro* HeLa cervical cancer cells to explore their dual application for MRI /optical imaging and thermal therapy for cancer treatment.

2. Result and Discussion

Figure 1 illustrates the schematic representation for synthesis of MNAs@Dye-SiO2@SiO2. The main idea behind the approach is to spatially confine the formation of the RITC dye doped silica shell over MNAs and evaluate its performance for optical imaging, as T2 MRI contrast agent and magnetic hyperthermia in cancer cells. The MNAs were prepared by a modified polyol process.[2] Then, RITC doped silica shell over the MNA were prepared through a Stober's sol-gel method using cetyltrimethylammonium bromide (CTAB) as an organic template.[6,7]The surface morphologies of MNAs and MNAs@Dye-SiO2@SiO2 were observed by high-resolution transmission electron microscopy (HR-TEM) images (**Fig-2a,c**).The MNAs are spherical, monodisperse and porous in nature. The Energy-dispersive X-ray spectroscopy (EDX) analysis shows the elemental composition of Mn and Fe, confirming the stoichiometry of MNAs (**Fig-2b**).The MNAs@Dye-SiO2@SiO2 too retains the similar morphological features of pure MNAs.

The MNAs cores are black spheres with an average size of around ~50 nm (**S.I.Figure-**1), and the grey silica shell shows an average thickness ~15-20nm.(**Figure-**2c) This core shell structure of MNAs@Dye-SiO2@SiO2 clearly visible by the difference of electrons permeability of MNAs and silica shell(**Figure-**2c). The overall size of MNAs@Dye-SiO2@SiO2 falls in between 60-80 nm, which is within the size range recommended for drug or gene delivery applications.[7,8] The crystal structure of the as synthesized MNAs was investigated using X-ray diffraction (XRD, **S.I.Figure**-2a). The MNAs crystallizes in inverse spinel magnetite structure of Fe_3O_4. The characteristic diffraction peaks are indexed as (220), (311), (400), (422), (611), and (440) planes following the standard data (JCPDS card 19-0629). The structure is not changed because of the similar ionic radii of Mn^{2+} and Fe^{2+}. However, a slight shift (towards lower 2theta) in position with respect to that of Fe_3O_4 is observed due to lattice strain.The (311) peak was further analyzed by fitting it to a Gaussian distribution to obtain its full width at half-maximum (FWHM; **S.I.Figure-**2a). The average crystallite size was estimated as~11.3 nm using Debye–Scherer equation. The formation mechanism of MNAs as described in the earlier reports follows two-stage growth process. First the precursor attained the supersaturating temperature for nucleation, and then primary nanoparticles start nucleating to a form aggregate at high temperature.[2,4]

$MnFe_2O_4$ nanoparticles is reported to have a high magnetization in comparison to most other ferrites.[1] The heating efficiency under a.c magnetic field and MRI contrast enhancement of magnetic nanoparticles increases with magnetization.[18] The magnetization plots of MNAs and MNAs@Dye-SiO2@SiO2 was determined at 300K (**S.I.Figure-**2b), exhibit superparamagnetic behaviour with the highest magnetization (M_s) value of 90.43 emu/g, and 62.45 emu/g (Mn+Fe) respectively, the former is higher as compared to the Fe_3O_4

nanoassemblies (~65emu/g).[2]The same phenomenon of high magnetization was also observed with other assemblies of MNPs.[19,20] The reason for a high M_s value in $MnFe_2O_4$ as described in the earlier reports is due to the partial substitution of Mn^{2+} at the tetrahedral sites in the spinel structure, which modulates the antiferromagnetic coupling interactions between the magnetic ions in the octahedral and tetrahedral sites resulting in the increase of the net magnetization of the nanoparticles[18,21]The N_2 adsorption-desorption isotherms exhibit a characteristic type IV isotherm with H_1-hysteresis loops, demonstrating their mesoporous characteristics (**S.I.Figure-**2c).[2,4] The average pore diameter calculated using the Barrett-Joiner-Halenda (BJH) method was 3.3 nm, and the Brunauer-Emmett-Teller (BET) surface area and total pore volume measured to be 175.3 m^2 g^{-1}, and 0.35 cm^3 g^{-1}, respectively. The nanostructure with high surface area, large pore volume, and uniform accessible mesopores demonstrated as potential nanocarrier for cancer diagnosis and therapy.[22,23] In order to demonstrate a highly permeable nature of silica shell, MNAs@Dye-SiO2@SiO2 were dispersed in an acetate buffer solution (pH 4.0) and stirred for 4 h to etch away the MNAs core. **Figure-**2d, shows the TEM image of hollow silica nanoparticles formed after dissolution of magnetic core in acidic buffer solution (pH 4.0). This confirms the mesoporous nature of MNAs@Dye-SiO2@SiO2.

The MTT assay was performed to determine the viability of HeLa cells after incubation with different concentrations of MNAs@Dye-SiO2@SiO2 for 24 and 48h of time period.(**S.I.Figure**3). The viability of control cells (without MNAs@Dye-SiO2@SiO2) was assumed to be 100%. We have observed cells viability of about 90% as compared to the control cells even at the higher concentration of metal ions (600µg, Mn+Fe/mL) after 24h incubation. These results clearly indicate that MNAs@Dye-SiO2@SiO2 have low

cytotoxicity. To demonstrate the optical imaging functionality of MNAs@Dye-SiO2@SiO2, the cellular uptake was observed by fluorescence microscopy. **Figure 3-a,b**, shows the confocal images of HeLa cells containing the red fluorescent granulated particles dispersed homogenously in the cell cytoplasm, which confirm the uptake of MNAs@Dye-SiO2@SiO2 by HeLa cells after 24 h of incubation. The uptake results confirmed the optical imaging efficacy of MNAs@Dye-SiO2@SiO2.

The next step was to evaluate their efficacy as a potential T2 MRI contrast agents. In MRI, superparamagnetic nanoparticles generate a strong magnetic field in homogeneities around the vicinity of water molecules to accelerate the relaxation of the water proton (^{1}H) magnetization.[19,21] We have determined the longitudinal (r_1) and transverse (r_2) relaxivities of MNAs@Dye-SiO2@SiO2 in agar phantom using a a 9.4 Tesla vertical-bore MRI scanner.[3] **Figure 4a,b** shows the inverse relaxation times, $1/T_1$ and $1/T_2$, as a function of the molar concentration of (Fe+Mn). It was observed that the inverse relaxation times varied linearly with the (Fe+Mn) concentration and the slope is defined as the longitudinal (r_1) and transverse (r_2) relaxivities, respectively. Based on classical relaxation model, the small size (<100nm) MNAs@Dye-SiO2@SiO2 nanoparticles fall within the size range of static dephasing regimes (SDR).[24,25] In the SDR, nanoparticles are predicted to exhibit the highest r_2 relaxivity, which is independent of their size. The r_2 value of the nanoparticle in the SDR regimes is determined by the equation:[26] (1)

$$r_2 = \frac{8\pi^2\sqrt{3}}{81}\frac{A^3 N_0}{10^6 Z}\gamma M s$$

Where A is the lattice parameter, N_0 is the Avogadro constant, Z is the number of formula units per unit cell, γ is the 2.67513×10^8 rad·s^{-1}·T^{-1} the gyromagnetic factor of the proton,

and M_s is the saturation magnetization. The r_1 of the synthesized MNAs@Dye-SiO2@SiO2 was measured to be 9.6±0.4 $s^{-1}mM^{-1}$ (Fe+Mn), which is smaller than that of commercially available contrast agents like ferucarbotran, resovist (12.3 ± 0.4 $s^{-1}mM^{-1}Fe$, 25.40 $s^{-1}mM^{-1}Fe$, **Figure 4a**).[27,28] But, a high r_2 value of 596±2 $s^{-1}mM^{-1}$ (Fe+Mn) was measured for MNAs@Dye-SiO2@SiO2,which is larger than those of commercially available ferucarbotran and resovist (239±2 $s^{-1}mM^{-1}$, 151.95 $s^{-1}mM^{-1}$, **Figure 4b**)[28,29] The relaxivity ratio, (r_2/r_1>10), is another important aspect to evaluate the efficiency of T_2-type contrast agents.[24,25]For MNAs@Dye-SiO2@SiO2 the r_2/r_1 ratio is calculated to be about 56, which is larger than that of ferucarbotran (19) and Resovist (5.90).[24,25] The pronounced longitudinal relaxivity and high r_2 / r_1 ratio of 56 of our MNAs@Dye-SiO2@SiO2 suggest their potential as T_2 negative contrast agents. The high relaxivity value of MNAs@Dye-SiO2@SiO2 correlates well with the recently demonstrated enhanced r_2 value of manganese ferrites nanocluster embedded in a substrate matrix of polymer vesicles or silica shell.[29,30,31]Yoon *et al* reported high r_2 relaxivity value (695 $s^{-1}mM^{-1}$ Mn+Fe) of silica coated manganese (Mn)-doped ferrite nanoclusters, which is close to the theoretical limit (759 $s^{-1}mM^{-1}Fe$).[25] In another approach, Qi *et al* assembled $Mn_{(0.05)}Fe_{(1-0.05)}Fe_2O_4$ nanoclusters by silane ligand-exchange reaction and showed the highest relaxivity value of 528 (Mn + Fe) mM^{-1} s^{-1}.[20]

It has been demonstrated that the surface coating on MNPs have influential role in enhancing the relaxivity through minimizing the effects of surface oxidation, magnetic disorder or spin canting [24,32]However, studies have also shown that the relaxivity depend on water diffusion based on the nature and thickness of coating material.[29,30,31]The mesoporous nature of MNAs are also advantageous to enhance MRI sensitivity by allowing the dipolar interactions between the magnetic moment of the particle and the surrounding water protons, which contribute to

the shortening of the T_2 relaxation time and dephasing of proton.[25,27]This allows more metal ions to be exposed to water molecules at the inner surface. The strength of MNAs@DyMNAs@Dye-SiO2@SiO2 as a positive contrast agent was also confirmed in MRI images of agar phantom with different concentration (from 20 to 100 µg mL^{-1}in terms of metal ions). The labeling efficacy of MNAs@Dye-SiO2@SiO2 was demonstrated with HeLa cells. The MNAs@Dye-SiO2@SiO2 labeled HeLa cells were dispersed in agarose gel to image on the 9.4 T MRI scanner. As it is evident from **Figure 4d** the concentration-dependent signal enhancement (dark-contrast in the T_2-weighted image) was observed in the MRI images of HeLa cells treated with MNAs@Dye-SiO2@SiO2compared with untreated cancer cells. Lartigue *et al* also observed the increase in signal intensity of multicore iron oxide labelled A549 cells in agarose gel.[19]Our results confirmed the efficacy of MNAs@Dye-SiO2@SiO2 as potential MRI nanoprobes for cancer diagnosis or cell labelling in stem cell therapy.

Previously, the silica encapsulated magnetic nanoparticles have been used for cancer hyperthermia.[33] We have also evaluated the heating efficacy of MNAs@Dy-SiO2@SiO2 for magnetic hyperthermia.The SAR value of MNAs@Dy-SiO2@SiO2 was measured over a wide range of magnetic field amplitudes at a constant frequency of 250 kHz (**Figure 5a**).The SAR value of MNAs@Dye-SiO2@SiO2 dispersed in PBS (conc. 0.5 mg/mL in terms of metal ions) reaches 375 ± 20 $W{\cdot}g^{-1}$, 330±15 $W{\cdot}g^{-1}$, 218 ±30 $W{\cdot}g^{-1}$under an external magnetic field of 33.3 kA/m^{-1}, 26 kA/m^{-1}, 13.3 kA/m^{-1}at a constant frequency of 250 kHz (**Figure 5a**). This shows the dependence of SAR on the various parameters such as saturation magnetization, applied a.c magnetic field strength and frequency.[19,34]The SAR value of MNAs@Dye-SiO2@SiO2 increases proportionally to the magnetic field strength as reported

by Lartigue *et al* for multicore iron oxide nanoparticle and Guardia *et al* for 19nm iron oxide nanocubes [19,35] To evaluate the heating effect on cancer cells, the cells pellet with a concentrations of $2x10^6$ in a 1 mL aqueous suspension of MNAs@Dye-SiO2@SiO2 (0.5 mg/mL ~in terms of metal ions concentration Mn+Fe at H=13.3kAm^{-1},f = 250kHz, *Hf* factor = $3.3x10^9$ Am^{-1}s^{-1}), was thermally activated for 30 min at a temperature in between 42ºC-45ºC. Generally, it has been demonstrated the safe range of applied ac magnetic fields where the product *H.f* does not exceed $5x10^9$Am^{-1} s^{-1} at clinical level for human body.[36,37] We have performed the magnetic hyperthermia in cancer cells relatively small *H.f* value ($3.3x10^9$Am^{-1} s^{-1}), it was agreeable that the hyperthermia treatment with MNAs@Dye-SiO2@SiO2 could be administered at a safe and tolerable range of *Hf* factor without any toxic or deleterious side effect. The MTT assay was performed to determine the cell viability with and without magnetic hyperthermia. The heating effect of MNAs@Dye-SiO2@SiO2 caused ~80-85 % of cancer cell death with respect to control cells (**Figure 5-b**). The **S.I.Figure 4-i,ii** shows the phase contrast images of control HeLa cell and MHT treated cells. The HeLa cells show complete distortion of cell membrane after MHT treatment in comparison to control cells. This revealed that the observed anticancer activity did not originate from the magnetic targeting of MNAs@Dye-SiO2@SiO2 to the cells, but was due to their induced heating effects. The same phenomenon of cell death was observed by Prasad *et al* using γ-$Mn_xFe_{2-x}O_3$ nanoparticles in HeLa cancer cell and Bae *et al* in human lung carcinoma A549 cells with chitosan coated ferrimagnetic iron oxide cube nanoparticles.[38,39] Furthermore, to confirm the cell death through apoptosis, the cancer cells were stained with Phalloidin-tetramethylrhodamine-B-isothiocyanate for actin filaments and nucleus by 4,6-diamidino-2-phenylindole dye (DAPI). The morphology of control and heat treated cells were imaged by a confocal microscopy

(**Figure 5c-i,ii**).The confocal image clearly shows the apoptosis of cancer cells through cell membrane blebbing, distortion of actin filaments and denaturation of nuclear compartment (**Figure 5c-i-ii**). These are the prominent morphological markers of apoptosis in cells. Yoo *et al* also demonstrated the same phenomenon of hyperthermia mediated cancer cell death caused through apoptosis rather than the necrosis.[40]These imply that the present superparamagnetic MNAs@Dye-SiO2@SiO2 nanocomposite combined with its functionality of magnetic hyperthermia, would be a potential theranostic agent for simultaneous optical/MR imaging and thermal therapy for cancer treatment.

Conclusions:

In summary, MNAs@Dye-SiO2@SiO2 represents a facile strategy for the preparation of highly potent superparamagnetic, silica encapsulated $MnFe_2O_4$ nanoassemblies with fluorescent dyes. Compared with other magnetic nanoassemblies, MNAs@Dye-SiO2@SiO2 exhibited small size (<100nm), high colloidal stability, high saturation magnetization, low cytotoxicity, enhanced relaxivities for T2 MRI contrast imaging and enhanced SAR values for magnetic hyperthermia. The *in-vitro* studies with HeLa cells confirmed the efficacy of MNAs@Dye-SiO2@SiO2 for providing high T2 relaxivity and heat at a reduced dosage, fulfilling an essential requirement for the development of iron-oxide based cancer theranostics nano-system. Furthermore, the versatile surface functionality and encapsulation efficiency of silica matrix for other types of metallic nanoparticles or chemo-therapeutics will help in fabricating a more robust multifunctional theranostic nanosystem for cancer therapy.

2. Experimental Section

2.1 Reagents and Materials

All the chemicals were of analytical grade and used as received. iron(III) chloride hexahydrate ($FeCl_3.6H_2O$, 98.9%), manganese chloride(II) tetrahydrate ($MnCl_2.4H_2O$, 98%), tetraethyl orthosilicate (TEOS), 3-aminopropyltriethoxysilane (APTES, 98%), Rhodamine-B isothiocyanate (RITC, 99% Aldrich), cetyltrimethylammoniumbromide (CTAB, 99%), 3-(4,5-dimethyl-thiazol-2yl)-2,5-diphenyl tetrazolium bromide (MTT, 98%),phalloidin-tetramethylrhodamine B-isothiocyanate conjugates and 4,6-diamidino-2-phenylindole (DAPI, 98%) were purchased from Sigma-Aldrich Co. (St. Louis, MO, USA). Anhydrous sodium acetate and ethylene glycol (EG) were purchased from Merck Chemical Ltd. Dulbecco's modified eagle medium (DMEM), antibiotic and antimycotic solution were obtained from Hi-Media Ltd (Mumbai, India) and HeLa cancer cell lines were procured from National Centre of Cell Science (NCCS, Pune, India).All tissue culture plates and flasks were purchased from NUNC (USA). The Milli-Q water with a resistivity of 18.2 MΩcm was used for all experiments.

2.2 Synthesis of MNAs@Dy-SiO2@SiO2

The 0.10 g of MNAs (~50nm), synthesized by a modified polyol method, was ultrasonicated in 0.1 M HCl aqueous solution (20 mL) for 10 min.[2,7]After that the acid treated MNAs were homogeneously dispersed in a aqueous solution of ethanol (80 mL), DI water (20 mL) and cetyltrimethylammoniumbromide (0.35g, CTAB).The suspension was vigorously stirred for 30 min. After stirring, the concentrated aqueous ammonia solution (1.5 mL, 25 wt.%) was added to the suspension, followed by drop wise addition of tetraethyl orthosilicate (TEOS, 0.5mL) with 100 μL of APS-modified dye solution as described by Kim *etal*.[16]The whole reaction dispersion was stirred at room temperature for

12 h to form the silica shell over MNAs. For further silica coating, the products were separated by magnet and washed 2-3 times with ethanol and water alternatively, and then redispersed in a mixed solution of CTAB (0.2g), ethanol (80 mL), DI water (20 mL) and aqueous ammonia solution (1mL). After mixing homogeneously for 30 min, the TEOS (0.25mL) was then added drop wise to the solution with stirring. The synthesized products were separated using magnet, washed with ethanol and water alternatively to remove undesirable nonmagnetic by-products and dried in air at 80^{o}C for 24 h. The surfactant CTAB was removed by refluxing in acidic ethanolic solution (0.75 ml concentrated HCl /100 ml ethanol solution) for 4h.

2.3 Characterization techniques

Powder X-ray diffraction (XRD) patterns of the MNAs and SiO_2@MNAs were obtained on the PANalytical X'Pert PRO diffractometer (PW3040/60)with Cu Kα radiation (λ = 1.5405 Å) and a Ni filter. All patterns were recorded over the angular range $10 \leq 2\theta/\text{deg} \leq 80$ with a step size of $\Delta 2\theta = 0.02$. The nitrogen (N_2) adsorption–desorption isotherms and pore size distributions were measured with an accelerated surface area and porosimetry instrument (ASAP 2020, Micrometrics USA). The surface area was determined using the BET equation from the N_2 adsorption– desorption isotherms between P/P_0 = 0-0.2. Prior to measurement, the sample was degassed at 120 ºC for 6 h. Transmission electron microscopy (TEM) and energy dispersive X-ray (EDX) analyses were performed using a JEOL JEM-2100F electron microscope with an accelerating voltage of 200 keV. The sample was diluted in ethanol and drop cast onto the surface of a TEM grid (Ted Pella, Inc., Form var/Carbon 400 mesh).The particle size distribution was processed by Image-J software. The weight chemical analysis was performed using inductively coupled plasma-atomic emission

spectrometer (ICP-AES, ARCOS Germany). The analysis of sample was done in comparison with the ICP-AES standard (Sigma). Magnetic properties of the samples were measured by physical properties measurement system (PPMS, Quantum Design).The measurements were recorded between −20000 and 20000 Oe at 300 K. Hydrodynamic diameter and size distribution of particles were analysed by dynamic light scattering (DLS, Malvern Nano-ZS, l = 632.8 nm) with samples dispersed in milli-Q water. Simultaneously, the surface charge alteration of particles was probed by zeta potential (Malvern Nano-ZS).

2.4 *In vitro* cytotoxicity and uptake of MNAs@Dye-SiO2@SiO2

The HeLa cell line were cultured in 25 cm^2 tissue culture flask containing DMEM medium supplemented with 10% Fetal Bovine serum (FBS), 1% antibiotic antimycotic solution in a humidified incubator (37 °C, 5% CO_2). MTT assay was performed on HeLa cancer cells to evaluate the *in-vitro* cytotoxicity of the MNAs@Dy-SiO2@SiO2. The HeLa cells were seeded in a 96-well plate at density of 20,000 viable cells per well and incubated for 24 h at 37 °C to allow cell attachment. The cells were treated with various concentrations of MNAs@Dye-SiO2@SiO2 (25, 50, 100, and 200 μg mL^{-1} ~in terms of metal ions) and incubated for 24 h. The wells without the MNAs@Dye-SiO2@SiO2 treatment were used as control. At the interval of 24h, the cells were washed twice using PBS, then 20 μL of freshly prepared MTT solution (0.5 mg mL^{-1} in PBS-phosphate buffer saline 7.4) in 100 μL DMEM media was added into each well. The plates were incubated at 37 °C for 3 h. After removing the media, the MTT–formazan crystals were dissolved by adding 100 μl of Dimethyl sulfoxide (DMSO) into the each wells of plate. The plate was placed on a shaking table for 5 minutes to mix the formazan into the solvent. Plate was then incubated

for 3 h and the absorbance at 550 nm was quantified by a micro plate reader (Victor 3-V Multilabel Plate Reader, PerkinElmer, USA). The formazan dye generated by the live cells was proportional to the number of live cells. Cells without nanoparticles were considered as control. Results were quantified by manually subtracting the blank value from each value and normalized against the control values.The data were averaged from three experiments for each MNAs@Dye-SiO2@SiO2 concentrations.

2.5MNAs@Dye-SiO2@SiO2 cellular uptake study

The uptake of MNAs@Dye-SiO2@SiO2 by HeLa cancer cells were observed by confocal microscopy imaging. The HeLa cells were cultured in a 12 well chamber plate with culture medium (DMEM with L-glutamine, 10% FBS, 1% of Antibiotic-antimycotic solution) at 37 °C in 5% CO_2. The HeLa cells were seeded into chamber slides at density of 20,000 cells/well.After 24 h of incubation, the culture medium was replaced by fresh DMEM containingMNAs@Dye-SiO2@SiO2 at different metal ions concentrations. After 24 h of incubation in the presence of MNAs@Dy-SiO2@SiO2, each well was washed with 1 × PBS for three times, treated with 0.5 mL of 4% paraformaldehyde solution for 10 min to fix the cells, and followed by washing with 1 × PBS for three times. The cells were then mounted using Vectashield mounting medium and were imaged by using a confocal laser scanning microscope (CLSM, Olympus Fluoview, FV500, Tokyo, Japan). The fluorescent image was acquired at (λ_{ex} = 570 nm and λ_{em} = 590 nm) forrhodamine-B isothiocyanate (RITC). The 60X water immersion objective was used to acquire and analyze images using the Fluoview software (Olympus, Tokyo, Japan).

2.6 MRI relaxation properties of MNAs@Dye-SiO2@SiO2 using phantom agar gels.

Suspensions of MNAs@Dye-SiO2@SiO2 in the concentration range of 0–100 µg/mL (~ term of metal ions, Mn+Fe) were prepared in PBS. A 2.5% w/v agar solution was prepared by heating 250 mg of agar in 10 mL of PBS at 80°C for 20 min.[3] For preparing phantom gels, 160 µL of the above agar solution was mixed with 840 µL of MNAs@Dye-SiO2@SiO2 suspension at each concentration, and was preheated to 60°C to prevent gelation while mixing. MNAs@Dye-SiO2@SiO2 and agar gel were mixed thoroughly in the warm condition in a 1.5 mL centrifuge tubes by turning the tubes upside down repeatedly. An aliquot of 250 µL of this mixture was transferred quickly to a 1.5mL micro-centrifuge tube and then allowed to cool to room temperature.

MRI experiments were performed at a 9.4 T (400 MHz for protons) 89 mm vertical-bore MRI scanner (Agilent, Santa Clara, CA) equipped with triple axis gradients (maximum strength 100 G/cm) and a 10 mm transmit/receive RF coil. T_1 and T_2 relaxation times for the samples were obtained using a multi-echo-spin-echo sequence (MEMS). For measuring the T_1 relaxation, 12 repetition times (TR) arrayed exponentially from 50 to 4000 ms. The other parameters were used for measuring the T_1 relaxations were Echo Time (TE) =8.4 ms. NE=1, field of view= 10×10 mm, thickness=1 mm, matrix, 128×128 pixels. T_2 relaxations were also obtained using a MEMS sequence with NE=32, TE=10ms, TR=4000, field of view = 10×10 mm, thickness =1 mm, matrix, 128×128 pixel. The Data were exported to Matlab software (Mathworks, Natick, MA) for calculating the relaxation times along with their T_1 and T_2 maps using a nonlinear regression algorithm. Then r_1 and r_2 relaxivities were calculated based on the slope of the linear regression of data points: ($1/T_1$ and $1/T_2$) (s^{-1}) versus metal ion concentrations.

2.7 *In-vitro* MR Imaging in HeLa cancer cells.

For *in-vitro* MR Imaging, HeLa cells were seeded in a six well plate in 2 mL of media for 24h. Subsequently, different concentrations of MNAs@Dye-SiO2@SiO2 (~ in terms of metal ions, Mn+Fe) 0, 25, and 100 µg/mL were added into each wells. The medium was removed after 24h and the cells were washed with PBS. The cells were detached using trypsin/EDTA and resuspended in DMEM media. The cell pellets were prepared by centrifugation at a speed of 2000 rpm for 5 min. The semisolid cell pellets were finally suspended in a 2% solution containing agarose and solidified at room temperature and then maintained at 4ºC. T_1 and T_2 relaxation maps were generated using multi-echo-spin-echo sequences (MEMS) acquired with the 9.4 T Agilent MRI scanners. T_1 relaxation data were generated by acquisitions of 12 MEMS images with TR exponentially arrayed between 50 ms and 4000 ms; effective echo time TE = 10 ms; number of echoes NE, 1; FOV= 10×10 mm; NEX=2; slice thickness=1 mm; using a 128 × 128 matrix. Parameters for measuring alteration of T_2 relaxation times were: TR, 4000 ms; effective echo time TE, 10 ms; number of echoes NE, 32; NEX, 2; FOV, 10×10 mm; matrix, 128×128 pixels; slice thickness, 1 mm). After acquisitions data were transferred to a PC and processes by a MATLAB code to generate T_1 and T_2 maps.

2.8 Hyperthermia Measurement.

The heat generating efficiency of MNAs@Dye-SiO2@SiO2 was performed by time-dependent calorimetric measurements using a RF generator (Easy Heat 8310, Ambrell, UK).In brief, 1mL of aqueous suspension of MNAs@Dye-SiO2@SiO2 at concentrations ranging from 0.2 to 1mg/mL (in terms of metals ions Mn+Fe) were subjected to varying magnetic field (13.3 kAm^{-1}, 26 kAm^{-1}, 33.3 kAm^{-1} with corresponding *H.f* factor, $3.3x10^9$ $Am^{-1}s^{-}$

[1], $6.5 \times 10^9 Am^{-1}s^{-1}$,$8.3 \times 10^9 Am^{-1}s^{-1}$) using RF generator operating at fixed frequency of 250 kHz. The time-dependent temperature rise was monitored using a fluoro-optic fibre thermometer (Luxtron, Corp).The specific absorption rate (SAR) was calculated using the following equation. (2)

$$SAR = C\frac{\Delta T}{\Delta t}\frac{1}{m_{Mn+Fe}}$$

Where, C is the specific heat of solvent (C_{water} = 4.18 Joule/gram °C), $\Delta T/\Delta t$ is the initial slope of the time-dependent temperature curve and m_{Mn+Fe} is the mass fraction of Mn+Fe in aqueous suspension.

2.9 Magnetic hyperthermia in cancer cells

The HeLa cells were subjected to magnetic hyperthermia treatment (MHT) by a modified protocol.[19] The HeLa cells were grown up to 90 % confluence in a 75 cm^2 culture flask. After 24 h, the DMEM medium was removed and the cell layer was washed three times with PBS, detached from substratum and centrifuge at 2000 rpm for 5 min to get cell pellet in a 15 ml sterile polypropylene tubes. Then, 2×10^6 HeLa cell were transferred into a 1mL DMEM medium containing 0.5mg/mL of MNAs@Dye-SiO2@SiO2 (~ in term of metal ions concentrations, Mn+Fe) in a 2 mL Eppendorf tube. The tubes were finally exposed to a magnetic hyperthermia setup (*H*=13.3kAm^{-1}, *Hf* factor = 3.3x10^9 A$m^{-1}s^{-1}$ at the center of 4-turn copper tubing coil, diameter = 6 cm)at a constant operating frequency of 250 kHz. When the temperature reached around in between 42-45 °C, the field was adjusted to maintain the temperature at 43 °C for 30 minute. For comparative study, HeLa cells were treated with MHT alone (without MNAs@Dy-SiO2@SiO2) and cells without any treatment were used as a control. After the thermal treatment, MNAs@Dye-SiO2@SiO2 was settled with magnet and supernatant was again removed and centrifuge to form cell pellet. The cells pellet was washed three times with PBS.

Then, 100 µl of 2 × 10^6 cells/mL were seeded in 96 well plates in 16 replicates for 24 h of incubation. The morphological feature of treated cell were observed by actin staining with Phalloidin-tetramethyl rhodamine-B-isothicyanate and nucleus by 4,6-diamidino-2-phenylindole (DAPI) according to the protocol of Sigma-Aldrich. The cell viability was determined by MTT (3-(4,5-Dimethyl-thiazol-2yl)-2,5-diphenyl tetrazolium bromide) assay as mentioned in section 2.4. The absorbance was measured at 550 nm wavelength in a micro plate reader (Victor 3-V Multilabel Plate Reader, PerkinElmer, USA).

The percentage of cell viability was calculated using equation. (3)

$$Cell\ viability = \frac{Absorbance\ of\ the\ treated\ well\ with\ or\ without\ \text{MNAs@Dy-SiO2@SiO2}}{Absorbance\ of\ control} X100$$

Acknowledgements:

This work is supported by Nano-mission, Department of Science and Technology (DST) and Nanotechnology Section, Department of Information Technology (DIT), Govt. of India. I am sincerely thankful to Mr Asif S Khan for his assistance with magnetic hyperthermia experiment. Authors are also thankful to Centre for Research in Nanotechnology and Science (CRNTS), I.I.T Bombay for providing TEM and SEM, confocal microscopy facilities.

Figures:

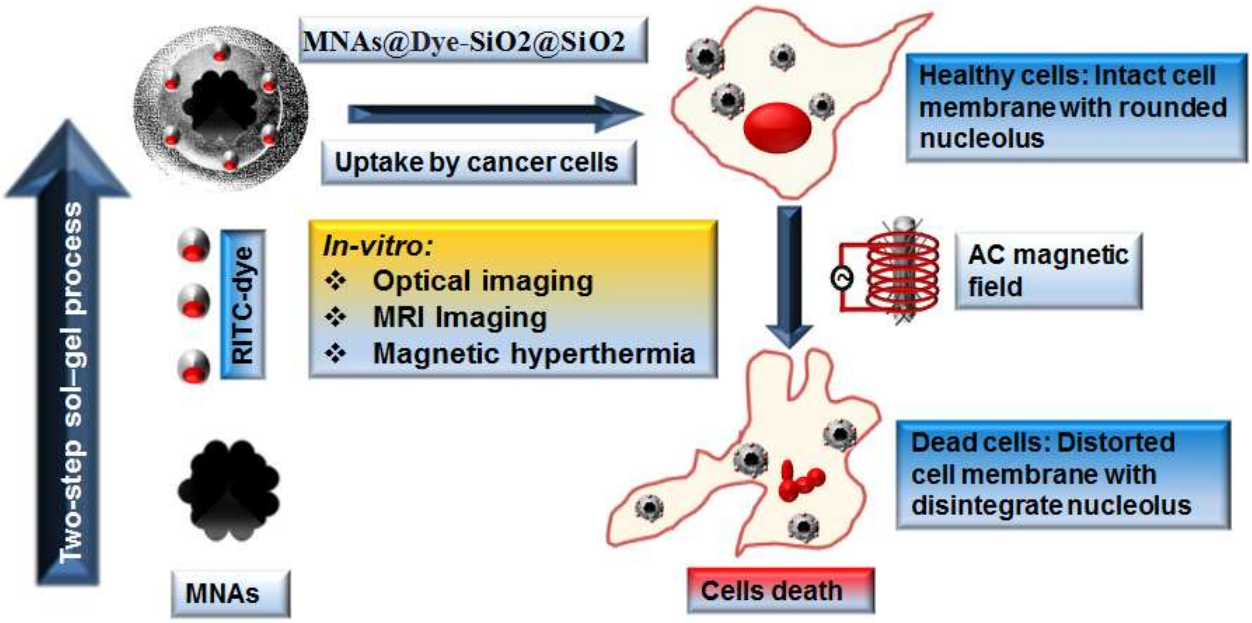

Figure.1 Schematic diagram shows the synthesis and theranostics application ofMNAs@Dye-SiO2@SiO2 for cancer therapy.

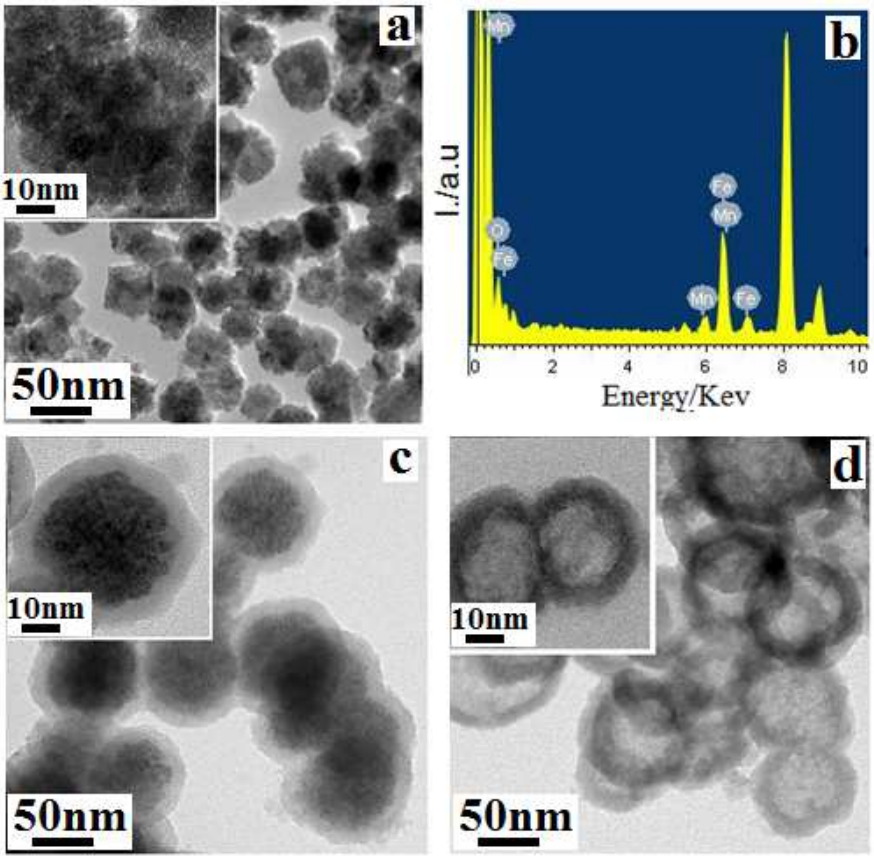

Figure 2(a) TEM images show the spherical morphology of MNAs and (b) EDX analysis for elemental composition confirms the presence of manganese, iron and oxygen (c) Silica coating over MNAs and (d) hollow silica sphere after dissolution of iron core in acidic buffer solution (pH 4) indicates the presence of mesoporous silica shell over MNAs. All insets show magnified images

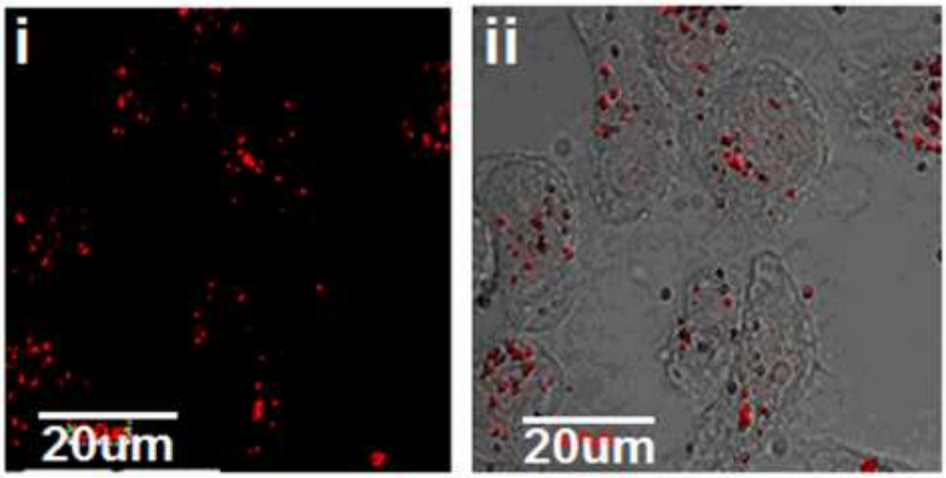

Figure. 3 (i,ii) show the confocal laser scanning microscopic (CLSM) images of HeLa cells with various concentrations of RITC-dye-dopedMNAs@Dye-SiO2@SiO2 after 24h of incubation. The spot-like red fluorescence inside cell cytoplasm shows the uptake of MNAs@Dy-SiO2@SiO2.

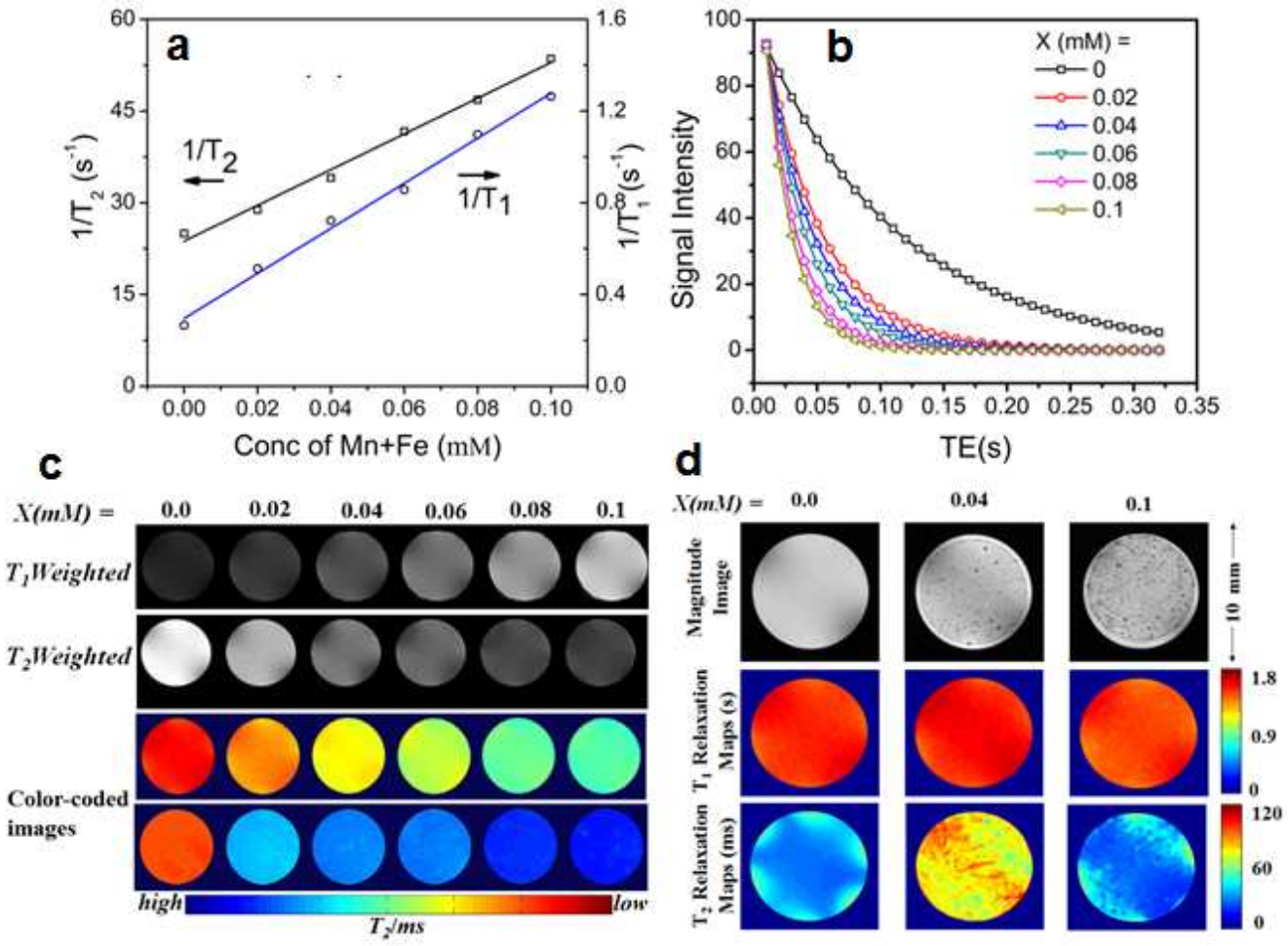

Figure 4a) Spin–lattice $1/T_1$and spin–spin $1/T_2$ relaxation rates of MNAs@Dye-SiO2@SiO2 at different metals ions concentrations (detonated X= (Mn+Fe). b) T_2 relaxation curves of various magnetic nanoparticle formulations in phantom agarose gel. (c) T_1- and T_2-weighted MR images of agarose phantoms at different concentrations of MNAs@Dye-SiO2@SiO2 and their respective color coded images. (d) T_2 weighted MR images of dispersed HeLa cell in agarose gel phantoms after 24 h of incubation with different concentrations of MNAs@Dy-SiO2@SiO2.

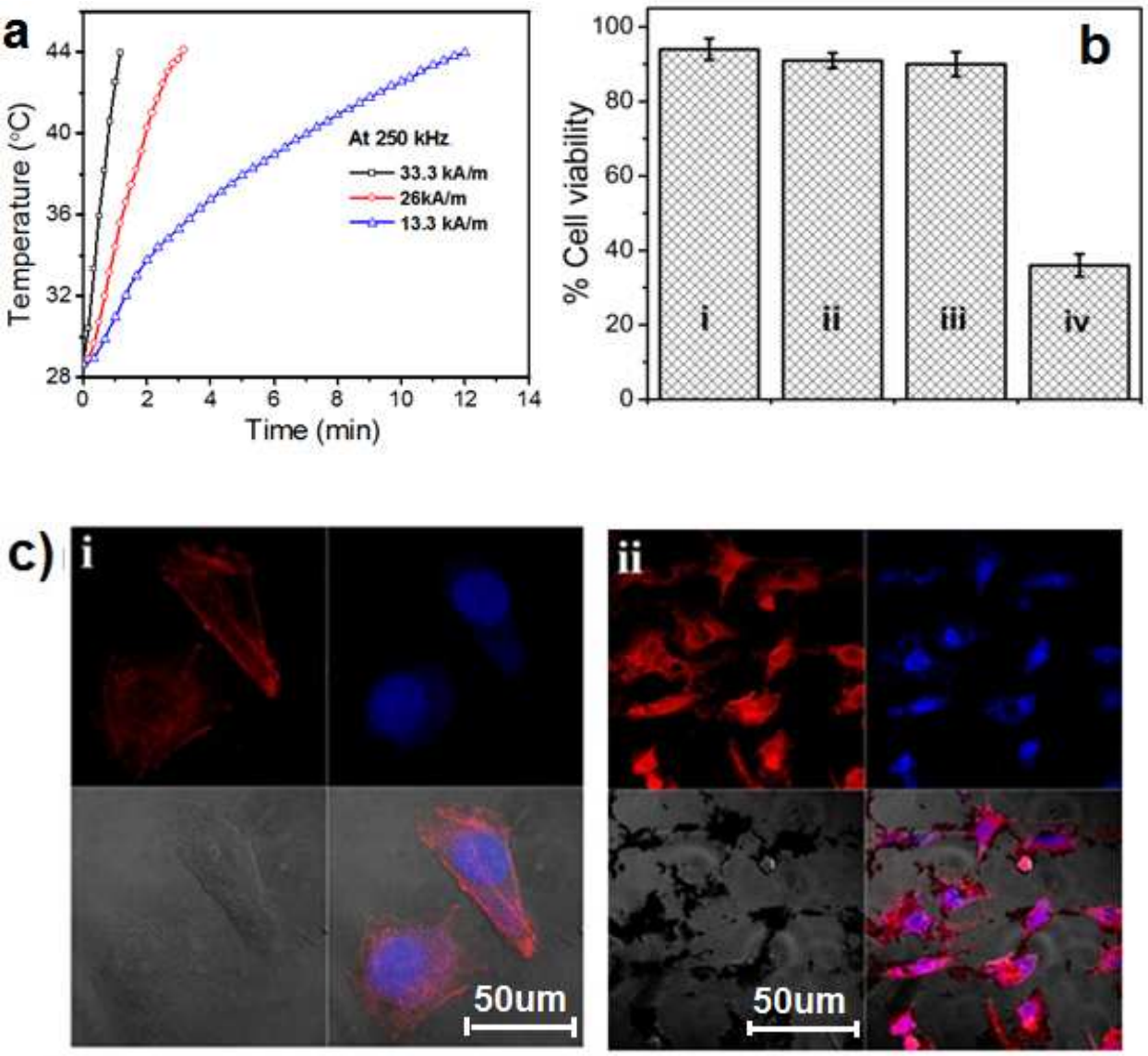

Figure 5. a) The calorimetric profile of MNAs@Dye-SiO2@SiO2 with respect to time. (b) Shows the quantitative estimation of cancer cell death by MTT assay (b-i) control HeLa cells, (b-ii) cell incubated with MNAs@Dy-SiO2@SiO2, w/o MHT, (b-iii) cells w/o MNAs@Dye-SiO2@SiO2 with MHT treatment (b-iv) with both MNAs@Dye-SiO2@SiO2 and MHT treatment. c-i) confocal images of control HeLa cells without MHT or MNAs@Dye-SiO2@SiO2 and ii) MHT-induced cancer cell death, shows the loss of cell-membrane integrity, membrane shrinkage and disintegration of the genetic materials and the nucleus, a morphological indication of cell apoptosis. The cancer cells were stained with Phalloidin-tetramethyl

rhodamine-B-isothiocyanate (red) for actin filaments and nuclei was stained by DAPI (4',6-diamidino-2-phenylindole; blue).

Reference:

(1) Yoo, D.; Lee, J.-H.; Shin, T.-H.; Cheon, J.:2011 Theranostic magnetic nanoparticles. *Acc. Chem. Res.***44**, 863-874.

(2) Barick, K. C.; Aslam, M.; Yen-Po, L.; Bahadur, D.; Pottumarthi, V. P.; Vinayak, P. D.: 2009Novel and efficient MR active aqueous colloidal Fe3O4 nanoassemblies. *J. Mater. Chem*., **19**, 7023-7029

(3) Yallapu, M.; Othman, S.; Curtis, E.; Gupta, B.; Jaggi, M.; Chauhan, S.:2011 Multi-functional magnetic nanoparticles for magnetic resonance imaging and cancer therapy. *Biomaterials*, **32**, 1890-1905.

(4) Kumar, S.; Daverey, A.; Sahu, N.K .; Bahadur, D.: 2013 In vitro evaluation of PEGylated mesoporous $MgFe_2O_4$ magnetic nanoassemblies (MMNs) for chemo-thermal therapy. *J.Mater. Chem. B*,**1**, 3652-3660.

(5) Dutz, S.; Hergt, R.:2014 Magnetic particle hyperthermia--a promising tumour therapy? *Nanotechnology*, **25**, 452001.

(6) Lee, J.; Lee, N.; Kim, H.; Kim, J.; Choi, S.; Kim, J.; Kim, T.; Song, I.; Park, S.; Moon, W.; Hyeon, T.:2010 Uniform mesoporous dye-doped silica nanoparticles decorated with multiple magnetite nanocrystals for simultaneous enhanced magnetic resonance imaging, fluorescence imaging, and drug delivery. *J. Am. Chem. Soc*., **132**, 552-557.

(7) Shili, G.; Piaoping, Y.; Chunxia, L.; Wenxin, W.; Yunlu, D.; Na, N.; Jun, L. 2010 Synthesis of Magnetic, Up-Conversion Luminescent, and Mesoporous Core-Shell-Structured Nanocomposites as Drug Carriers. *Adv. Funct. Mater*.,**20**.1166-1172.

(8) Chen, Y.; Chen, H.; Shi, J. 2013 In vivo bio-safety evaluations and diagnostic/therapeutic applications of chemically designed mesoporous silica nanoparticles. *Adv. Mater*.,**25**, 3144-3176.

(9) Gao, J.; Gu, H.; Xu, B.: 2009Multifunctional magnetic nanoparticles: design, synthesis, and biomedical applications. *Acc. Chem. Res.*, **42**, 1097-1107.

(10) Sailor, M. J.; Park, J. H.: 2012 Hybrid nanoparticles for detection and treatment of cancer. *Adv Mater*,**24**, 3779-802.

(11) Lee, J. E.; Lee, N.; Kim, T.; Kim, J.; 2011Hyeon, T.:Multifunctional mesoporous silica nanocomposite nanoparticles for theranostic applications. *Acc. Chem. Res.*, **44**, 893-*902.*

(12) Pohaku Mitchell, K.; Liberman, A.; Kummel, A.; Trogler, W.:2012Iron(III)-doped, silica nanoshells: a biodegradable form of silica. *J. Am. Chem. Soc*, **134**, 13997-14003.

(13) Insin, N.; Tracy, J. B.; Lee, H.; Zimmer, J. P.; Westervelt, R. M.; Bawendi, M. G.: 2008Incorporation of iron oxide nanoparticles and quantum dots into silica microspheres. *ACS nano*, **2**, 197-202.

(14) Zhang, F.; Braun, G. B.; Pallaoro, A.; Zhang, Y.; Shi, Y.; Cui, D.; Moskovits, M.; Zhao, D.; Stucky, G. D.: 2012Mesoporous multifunctional upconversion luminescent and magnetic "nanorattle" materials for targeted chemotherapy. *Nano letters*, **12**, 61-7.

(15) Montalti, M.; Prodi, L.; Rampazzo, E.; Zaccheroni, N.: 2014Dye-doped silica nanoparticles as luminescent organized systems for nanomedicine. *Chem Soc Rev*, **43**, 4243-68.

(16) Bae, S.; Tan, W.; Hong, J.-I.: 2012Fluorescent dye-doped silica nanoparticles: new tools for bioapplications. *Chemi. Commun.*, **48**, 2270-2282.

(17) Burns, A.; Ow, H.; Wiesner, U.: 2006,Fluorescent core-shell silica nanoparticles: towards "Lab on a Particle" architectures for nanobiotechnology. *Chem Soc Rev*, **35**, 1028-1042.

(18) Obaidat, I.; Issa, B.; Haik, Y.: 2015 Magnetic Properties of Magnetic Nanoparticles for Efficient Hyperthermia. *Nanomaterials*, **5**, 63-89.

(19) Lartigue, L.; Hugounenq, P.; Alloyeau, D.; Clarke, S.; Lévy, M.; Bacri, J.-C.; Bazzi, R.; Brougham, D.; Wilhelm, C.; Gazeau, F.: 2012 Cooperative organization in iron oxide multi-core nanoparticles potentiates their efficiency as heating mediators and MRI contrast agents.*ACS nano*,**6**, 10935-10949.

(20) Qi, Y.; Shao, C.; Gu, W.; Li, F.; Deng, Y.; Li, H.; Ye, L.2013Carboxylic silane-exchanged manganese ferrite nanoclusters with high relaxivity for magnetic resonance imaging. *J.Mater. Chem. B.*, **1**, 1846-1851.

(21) Jang, J.-t.; Nah, H.; Lee, J.-H.; Moon, S.; Kim, M.; Cheon, J.:2009Critical enhancements of MRI contrast and hyperthermic effects by dopant-controlled magnetic nanoparticles. *Angew. Chem., Int. Ed.*, **48**, 1234-1238.

(22) Xuan, S.; Wang, F.; Lai, J. M.; Sham, K. W.; Wang, Y. X.; Lee, S. F.; Yu, J. C.; Cheng, C. H.; Leung, K. C.: 2011Synthesis of biocompatible, mesoporous Fe(3)O(4) nano/microspheres with large surface area for magnetic resonance imaging and therapeutic applications. *ACS Appl.Mater. Interfaces*, **3**, 237-44.

(23) Xuan, S. H.; Lee, S. F.; Lau, J. T.; Zhu, X.; Wang, Y. X.; Wang, F.; Lai, J. M.; Sham, K. W.; Lo, P. C.; Yu, J. C.; Cheng, C. H.; Leung, K. C.: 2012Photocytotoxicity and magnetic relaxivity responses of dual-porous gamma-Fe2O3@meso-SiO2 microspheres. *ACS Appl.Mater. Interfaces*, **4**, 2033-40.

(24) Vuong, Q.; Berret, J.-F.; Fresnais, J.; Gossuin, Y.; Sandre, O.:2012A universal scaling law to predict the efficiency of magnetic nanoparticles as MRI T(2)-contrast agents. *Adv. Healthcare Mater.*, **1**, 502-512.

(25) Yoon, T.-J.; Lee, H.; Shao, H.; Hilderbrand, S.; Weissleder, R.:2011Multicore assemblies potentiate magnetic properties of biomagnetic nanoparticles. *Adv Mater*, **23**, 4793-4797.

(26) Lee, N.; Choi, Y.; Lee, Y.; Park, M.; Moon, W. K.; Choi, S. H.; Hyeon, T.:2012Water-dispersible ferrimagnetic iron oxide nanocubes with extremely high r(2) relaxivity for highly sensitive in vivo MRI of tumors. *Nano letters*, **12**, 3127-31.

(27) Li, L.; Jiang, W.; Luo, K.; Song, H.; Lan, F.; Wu, Y.; Gu, Z.:2013Superparamagnetic iron oxide nanoparticles as MRI contrast agents for non-invasive stem cell labeling and tracking. *Theranostics*, **3**, 595-615.

(28) Lee, N.; Hyeon, T.: 2012Designed synthesis of uniformly sized iron oxide nanoparticles for efficient magnetic resonance imaging contrast agents. *Chem Soc Rev*,**41**, 2575-2589.

(29) LaConte, L.; Nitin, N.; Zurkiya, O.; Caruntu, D.; O'Connor, C.; Hu, X.; Bao, G.: 2007Coating thickness of magnetic iron oxide nanoparticles affects R2 relaxivity. *J Magn Reson Imaging*., **26**, 1634-1641.

(30) Pinho, S.; Pereira, G.; Voisin, P.; Kassem, J.; Bouchaud, V.; Etienne, L.; Peters, J.; Carlos, L.; Mornet, S.; Geraldes, C.; Rocha, J.; Delville, M.-H.: 2010Fine tuning of the relaxometry of γ-$Fe2O_3$@SiO_2 nanoparticles by tweaking the silica coating thickness. *ACS nano*, **4**, 5339-5349.

(31) Pöselt, E.; Kloust, H.; Tromsdorf, U.; Janschel, M.; Hahn, C.; Maßlo, C.; Weller, H.: 2012Relaxivity optimization of a PEGylated iron-oxide-based negative magnetic resonance contrast agent for T_2-weighted spin-echo imaging. *ACS nano, **6**,* 1619-1624.

(32) Brooks, R.: 2002 T(2)-shortening by strongly magnetized spheres: a chemical exchange model. *Magn. Reson.Med*, **47**, 388-391.

(33) Martin-Saavedra, F. M.; Ruiz-Hernandez, E.; Bore, A.; Arcos, D.; Vallet-Regi, M.; Vilaboa, N.: 2010 Magnetic mesoporous silica spheres for hyperthermia therapy. *Acta Biomaterialia*, **6**, 4522-31.

(34) Dutz, S.; Hergt, R.: 2013 Magnetic nanoparticle heating and heat transfer on a microscale:Basic principles, realities and physical limitations of hyperthermia for tumour therapy. *Int. J. Hyperthermia*, **29**.790-800.

(35) Mamiya, H.; Jeyadevan, B.: 2011 Hyperthermic effects of dissipative structures of magnetic nanoparticles in large alternating magnetic fields. *Sci Rep*, **1**, 157.

(36) Hergt, R.; Dutz, S.; Roder, M.: 2008 Effects of size distribution on hysteresis losses of magnetic nanoparticles for hyperthermia. *Journal of physics. Condensed matter*,**20**, 385214.

(37) Guardia, P.; Di Corato, R.; Lartigue, L.; Wilhelm, C.; Espinosa, A.; Garcia-Hernandez, M.; Gazeau, F.; Manna, L.; Pellegrino, T.:2012 Water-soluble iron oxide nanocubes with high values of specific absorption rate for cancer cell hyperthermia treatment. *ACS nano*, **6**, 3080-3091.

(38) Prasad, N. K.; Rathinasamy, K.; Panda, D.; Bahadur, D.: 2007Mechanism of cell death induced by magnetic hyperthermia with nanoparticles of γ-MnxFe2–xO3 synthesized by a single step process. *J. Mater. Chem.*,**17**.5042-5051.

(39) Bae, K.; Park, M.; Do, M.; Lee, N.; Ryu, J.; Kim, G.; Kim, C.; Park, T.; Hyeon, T.:2012Chitosan oligosaccharide-stabilized ferrimagnetic iron oxide nanocubes for magnetically modulated cancer hyperthermia. *ACS nano*,**6**, 5266-5273.

(40) Yoo, D.; Jeong, H.; Noh, S. H.; Lee, J. H.; Cheon, J.: 2013 Magnetically triggered dual functional nanoparticles for resistance-free apoptotic hyperthermia. *Angew Chem Int Ed Engl*, **52**, 13047-51.

Theranostics fluorescent silica encapsulated magnetic nanoassemblies for *in-vitro* MRI imaging and hyperthermia

Sunil Kumar[a], Amita Daverey[b,c] Vahid Khalilzad-Sharghi[d], Niroj K. Sahu[b], Srivatsan Kidambi[c], Shadi F. Othman[d] and Dhirendra Bahadur[b]*

*[a]Department of Chemical Engineering [b]Department of Metallurgical Engineering and Materials Science, Indian Institute of Technology Mumbai-400076, India. [c]Department of Chemical and Bimolecular Engineering, [d]Department of Biological Systems Engineering, University of Nebraska, Lincoln, NE-68588. USA.*E-mail: dhirenb@iitb.ac.in Tel: +91 22 25767632, Fax: +91 22 2576 3480.*

Graphical Abstract: